DOI 10.1515/hf-2013-0189 — Holzforschung 2014; 68(8): 941–949

Sebastian Clauß, Corina Pescatore and Peter Niemz*

Anisotropic elastic properties of common ash (*Fraxinus excelsior* L.)

Abstract: Hardwoods in principle show a similar orthotropic behavior as softwoods; however, the ratios of the mechanical parameters between the three anatomical directions and their magnitudes are different and depend strongly on the individual microstructure of the species. The aim of the current study was to characterize the 3-D elastic behavior of common ash (*Fraxinus excelsior* L.) by tensile, compression, and shear tests in the three anatomical directions and stepwise in between, by means of a universal testing machine in combination with a digital image correlation technique. Young's moduli, shear moduli, and Poisson's ratios have been determined for the different load directions. From studies on the radial-tangential plane of other wood species, it is known that the elastic moduli in the principal directions and the off-axis elastic moduli vary in a nonlinear correlation, depending on density gradients between earlywood and latewood. This angular dependency has been experimentally and theoretically proven for ash. Furthermore, the dependency of mechanical parameters on the fiber-load angle has been experimentally determined. The measurements for principal and off-axis load directions provide a sound basis for modeling of hardwood structures.

Keywords: anisotropy, ash, grain angle, orthotropic properties, ring angle, shear modulus, Young's modulus

***Corresponding author: Peter Niemz,** Institute for Building Materials, ETH Zurich, Stefano-Franscini-Platz 3, CH-8093 Zurich, Tel.: (+41) 44-63-25230, Fax: (+41) 44-63-21174, e-mail: niemzp@ethz.ch
Sebastian Clauß and Corina Pescatore: Institute for Building Materials, ETH Zurich, Switzerland

Introduction

In general, the material behavior of wood has been widely investigated. Based on solid state physics, the 3-D elastic material behavior can be described based on the compliance matrix for orthotropic materials (Eq. 1) with the engineering elastic parameters ε_{ii} and γ_{ij} being the normal and shear strains, σ_{ii} and τ_{ij} being the normal and shear stresses, E_{ii} and G_{ij} being moduli of elasticity (MOE) and shear, and finally the Poisson's ratios ν_{ij}, respectively. In the case of wood, the mechanical properties differ significantly within the longitudinal (L), radial (R), and tangential (T) directions. However, the anisotropic behavior of wood is individual and depends strongly on its anatomical structure.

$$\begin{bmatrix} \varepsilon_L \\ \varepsilon_R \\ \varepsilon_T \\ \gamma_{LR} \\ \gamma_{LT} \\ \gamma_{RT} \end{bmatrix} = \begin{bmatrix} \frac{1}{E_L} & \frac{-\nu_{LR}}{E_R} & \frac{-\nu_{LT}}{E_T} & 0 & 0 & 0 \\ \frac{-\nu_{RL}}{E_L} & \frac{1}{E_R} & \frac{-\nu_{RT}}{E_T} & 0 & 0 & 0 \\ \frac{-\nu_{TL}}{E_L} & \frac{-\nu_{TR}}{E_R} & \frac{1}{E_T} & 0 & 0 & 0 \\ 0 & 0 & 0 & \frac{1}{G_{LR}} & 0 & 0 \\ 0 & 0 & 0 & 0 & \frac{1}{G_{LT}} & 0 \\ 0 & 0 & 0 & 0 & 0 & \frac{1}{G_{RT}} \end{bmatrix} \begin{bmatrix} \sigma_L \\ \sigma_R \\ \sigma_T \\ \tau_{LR} \\ \tau_{LT} \\ \tau_{RT} \end{bmatrix} \quad (1)$$

First and foremost, the difference between the L direction and the directions perpendicular to the grain is evident, whereas the stiffness in the L direction is about 10–20 times higher than in the R and T directions. As the L direction predominantly determines most kinds of structural applications of wood, information about values of strength and stiffness in that direction is well available in the literature. Selected parameters of ash and other hardwoods have been published by Baumann (1922), Stamer (1935), Kollmann (1941, 1951), Kühne (1951), Leclerco (1975), Bodig and Jayne (1993), Sliker and Yu (1993), Szalai (1994), Wagenführ (1996), Pozgaj et al. (1997), Sell (1997), DIN 68364 (2003), Bonoli et al. (2005), amongst others. A few authors also presented results obtained for the traverse directions of individual softwood and hardwood species, such as Hörig (1933), Wommelsdorf (1966), Neuhaus (1983), Keunecke et al. (2008), Hering et al. (2012), and Ozyhar et al. (2012). However, especially in the case of hardwoods, complete data sets for the three main anatomical directions

rarely exist that are sufficient for static calculations and modeling in wood construction, and for calculations on multilayered boards, parquet, or musical instruments with the finite element (FE) method. Several studies about grain angle dependencies were published, for example, by Hearmon and Barkas (1941), Suzuki and Sasaki (1990), Kabir et al. (1997), Reiterer and Stanzl-Tschegg (2001), Liu (2002), and Yoshihara (2009). A comprehensive work about grain and ring angle dependent compression strength and elasticity was presented by Lang et al. (2002), and the angle dependent elastic behavior within the *RT* plane of softwoods was investigated by Hearmon (1948), Kennedy (1968), and Garab et al. (2010).

It was demonstrated that softwood species in particular have a strong anisotropic behavior in the *RT* plane with the lowest stiffness in between the anatomical directions. The maximum values of compliance are reached at an angle of about 45° because of a comparable low shear modulus in the *RT* plane. However, yew wood reveals a different behavior with a much lower degree of anisotropy (Garab et al. 2010), comparable to theoretically determined values by Grimsel (1999), Hering et al. (2012), and Ozyhar et al. (2012), for hardwoods like beech. The calculations were conducted according to an approach described in Bodig and Jayne (1993), on the basis of works by Voigt (1928), and Hörig (1933). The greater variations in the density between earlywood and latewood are most likely responsible for the distinctive anisotropy of spruce and other comparable softwood species.

The drawback of previous approaches, however, was that results of different studies, or dynamic and static methods were combined to access the data needed for a comparison of numerical and experimental results. Mostly dynamic methods, measuring the ultrasound velocities, as described in Bucur (2006), were used to determine the shear moduli, and static tests were used to determine MOEs and Poisson's ratios.

In the current study, the stiffness of the material should be determined with increments of 15° in and between the anatomical directions in the fiber or growth ring angle, respectively, in tension and compression tests of the same samples, in the linear elastic region. In addition, the Poisson's ratios should be determined in all loading cases for the individual sectional planes. Furthermore, the shear moduli will be statically determined by an Arcan testing device for all configurations in the main anatomical directions. The expectation is that an objective comparison of numerical and experimental results will be possible from the data obtained.

Materials and methods

Tension and compression tests

The quasi-static determination of the MOE was performed under tension and compression load with the same specimens on a Zwick 100 (Zwick GmbH & Co. KG, Ulm, Germany) universal testing machine equipped with a 100 kN load cell (Figure 1a). A displacement-controlled test was performed with a testing speed of about 1 mm min^{-1}. In the compression test, a simply supported pressure plate was used to avoid bending effects on the specimen. The central load transmission in tension test for both configurations was achieved with conical clamp jaws.

For the strain measurement, an optical video image correlation system (VIC 2D, Correlated Solutions Inc., Columbia, SC, USA) was applied that allows an evaluation of the strain distribution over the complete specimen surface. To this purpose, an optimized correlation algorithm was available, which provided full-field displacement and strain data for mechanical testing on planar specimens. The in-plane movement was determined as a mean strain in the load direction and across this direction for the selected measurement area of interest with a size of about 11×11 mm^2 (Figure 1b), in between the parallel section of the specimen. The system can measure in-plane displacements and strains from 50 microstrains to 2000% strains and above. In the actual measurements, lateral strains in the *L* direction reach values under *T* load of about 0.015%. The specimen preparation only requires the application of a random speckle pattern.

The displacement data from each side of the specimen during the tension and compression measurements (in the same run) were determined by three cameras with a resolution of 2048×2048, and one with 1628×1236 pixels (models AVT Pike F421B and Dolphin F201b, Allied Vision Technologies, Stadtroda, Germany) (Figure 1a). The image capturing was synchronized with the load signal via an A/D converter. After testing all samples, the calculation of the strain data was performed in the linear range of 12.5–50% of the actual force at 0.2% plastic deformation ($F_{0.2}$) (Figure 1c), to ensure linear elastic behavior of the material. These orientation dependent maximum forces were determined in a preliminary test for the main directions with $F_{0.2(L)}$=60.0 MPa, $F_{0.2(R)}$=18.8 MPa, and $F_{0.2(T)}$=13.2 MPa. The forces in the *LR* and *LT* planes for the angles θ in between the main directions were calculated based on the Hankinson formula (Eq. 2) with an exponent n=2.5.

$$F_\theta = \frac{F_{0.2(L)} F_{0.2\left(\frac{R}{T}\right)}}{F_{0.2(L)} \sin^n \theta + F_{0.2\left(\frac{R}{T}\right)} \cos^n \theta}. \quad (2)$$

The strength in the *RT* plane varies as a sinusoidal function (Eq. 3) described in Bodig and Jayne (1993). The maximum forces in the *RT* plane with the empirical constant K=0.2 were calculated with this equation.

$$F_\theta = \frac{2}{\pi}(F_{0.2(R)} - F_{0.2(T)}) + \frac{K}{2}(-\sin 2\theta)(F_{0.2(R)} + F_{0.2(T)}). \quad (3)$$

The MOEs for the individual specimens were calculated from the stress-strain data for each specimen surface individually. From these values, an outlier test was performed excluding individual specimens with values lying outside the one and a half interquartile range of the complete sample. In several cases, bending effects led to differing values of the opposite cameras, however by averaging the values,

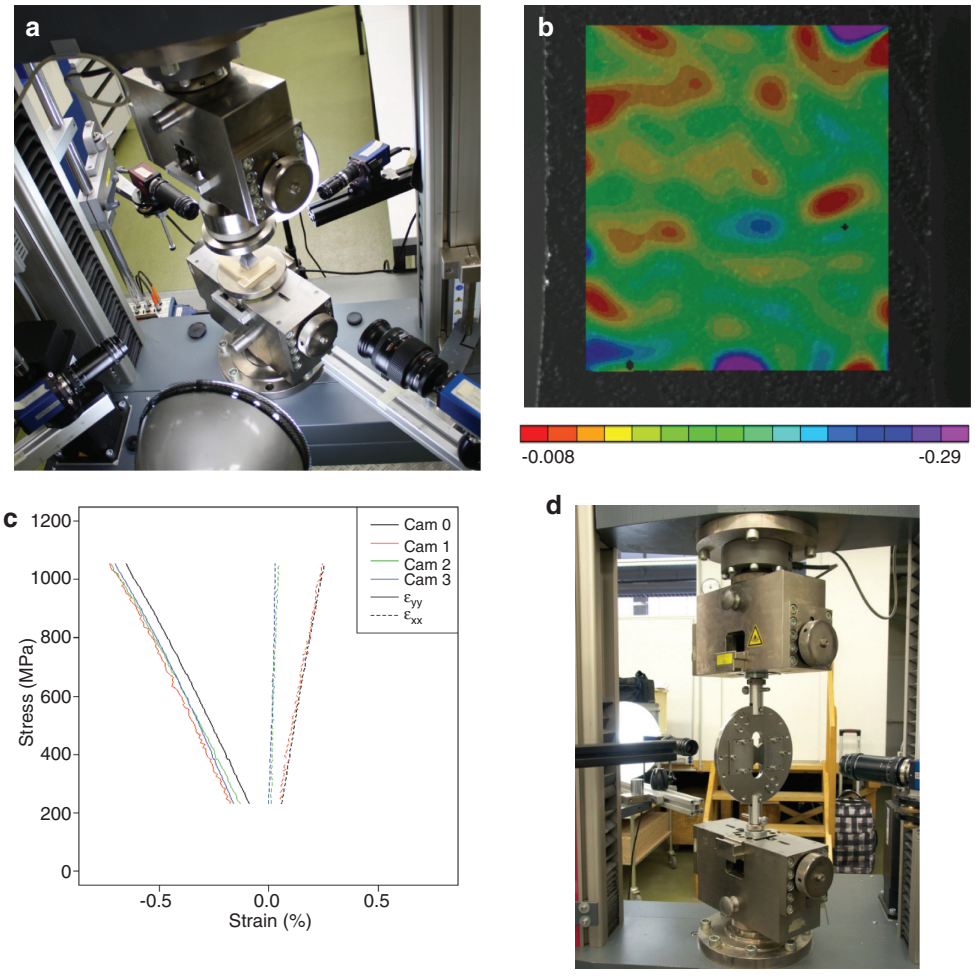

Figure 1 Test setup and data evaluation via video correlation.
(a) Tension-compression setup with four cameras. (b) Area of interest for VIC 2D analysis with strain distribution in percent. (c) Stress-strain diagram of a sample at compression load in the *T* direction with negative strain in *T* (ε_{yy}), and positive strain in the *R* and *L* directions (ε_{xx}). (d) Arcan test setup with two cameras.

the errors cancel out each other. From the reduced sample the mean value and variance was calculated.

Shear test

The measurement of the shear modulus was performed according to Arcan et al. (1978). The first application of this test was determining material properties of deformable material by Goldenberg et al. (1958), and it is based on the known Iosipescu test (Iosipescu 1967). A test design analogue to that applied by Xavier et al. (2009), was constructed (Figure 1d). The device consists of two inverted mirrored semicircles made of steel with a thickness of 10 mm, which fits frictionless through a key and slot connection. Several circumferential holes allow different force transmissions. The test was performed with a Zwick testing machine with a speed of 1 mm min^{-1}. The strain measurement was performed with the optical method described above with the help of two cameras capturing front and back simultaneously. The measurements were performed on six configurations resulting from the three orientations in the orthotropic material model. A mean was calculated for the three moduli of the compliance matrix from their corresponding values. The specimens were loaded in the linear elastic region up to the maximum force, which was determined in a preliminary test, where the specimens were loaded until failure. The maximum force for the *RT* and *TR* samples was 2 MPa, for the *TL* and *RL* samples it was 5 MPa, and for *LR* and *LT* samples it was 4 MPa. The shear strain was determined in an area of about 4 mm×20 mm.

Materials

Common ash (*Fraxinus excelsior* L.) was harvested near Zurich, Switzerland, with an average raw density of 0.60 g cm^{-3}, and an average moisture content (MC) of about 12%. All test specimens for the determination of the physical and mechanical properties were cut from the same trunk, however, only sapwood was taken for the investigation. All knots or defects in the wood structure were excluded from testing in advance.

Between the anatomical directions, specimens were cut with stepwise increasing fiber and growth ring angles, with an interval of 15°. In

total, 21 different configurations resulted that were tested at a normal climate (20°C/65 RH) only. As the angles deviated sometimes from the target angles, all fiber and growth ring angles of the individual specimens were measured optically by image analysis. The tension and compression tests were conducted on 95 mm long, dog-bone shaped specimens (Figure 2a). This shape allows transferring the forces at the clamps to the specimen without deformation in the *R* and *T* directions under *L* tensile load. At least 10 specimens were tested per individual direction. It is hardly possible to gather specimens with straight alignment of the growth rings over the whole length of the sample, especially in the *T* direction, therefore supports were glued on the boards made out of beech wood to obtain the desired specimen dimensions.

For the Arcan test specimens of the shape displayed in Figure 2b, (dimensions of 50×130 mm²) with a thickness of 8 mm were prepared. According to Hung and Liechti (1999), the notch was formed with an angle of about 110°, and a radius at the notch base of 2 mm. This geometry seems to be a good compromise for specimens of different orientations in the *TR*, *LR*, and *LT* planes.

Results and discussion

Modulus of elasticity

The results of the measurements are summarized for the tension and compression tests in the anatomical directions, and between them in steps of 15° (Table 1). For the three anatomical directions two mean values were derived, which belong to samples from different parts of the trunk. For the *L* and *T* orientations, these values correspond to each other with only small variations, which indicates that the position in the trunk is of minor importance, however, in the case of the radial samples tested, the variation was about 18%, without showing a difference in density or growth ring distance. The reason can be found in angle deviations up to about 15° in the *LR* plane of these samples that caused a decrease of the MOE in the *R* direction. The number of samples slightly varies in the different orientations caused by individual outliers and available samples. The mean values in the fiber directions reach MOEs of about 9.0 GPa in compression load, and about 8.3 GPa in tension load. The radial direction shows values of about 1.0 GPa in compression and tension load. The *T* direction reveals the lowest values with 0.6 GPa in compression and tension load. According to the results, no significant variation between the types of load was obtained which was already shown by Baumann (1922).

Baumann (1922) obtained slightly higher values in the *L* direction for the compression load. Comparing these results to other studies on ash (Table 2), the currently obtained values are significantly lower, depending on individual wood specific parameters. As is well known, the density particularly plays a major role regarding the mechanical properties. The results of the displayed values in Table 2 obviously show an increasing MOE with increasing density in the *L* direction. The directions perpendicular to the grain do not follow this correlation. On the whole, one can see a variation in the values of about

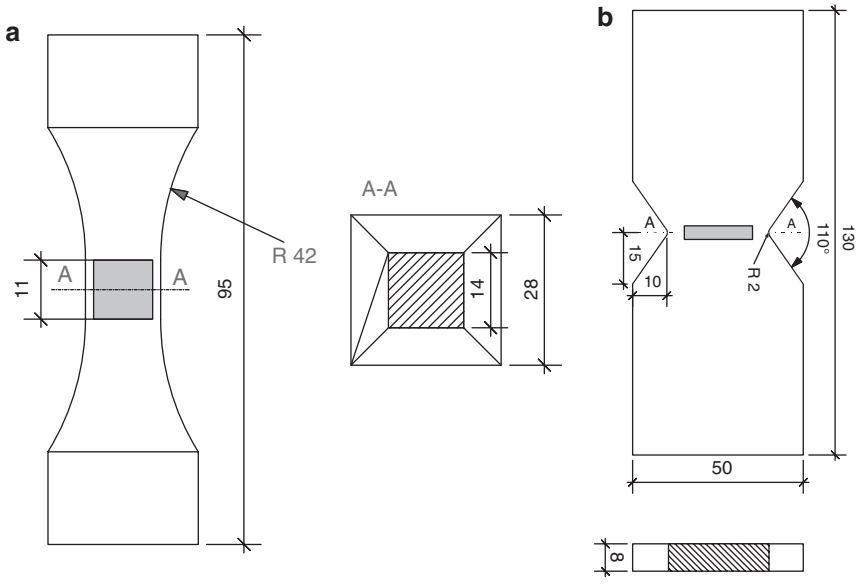

Figure 2 Specimen type and dimensions with the optical analyzed area displayed in gray. The dimensions are in (mm). (a) Dog-bone specimen. (b) Arcan specimen.

Table 1 Results of MOEs determined in tension and compression test with loading in and between the three anatomical directions *L*, *R*, *T* (ω=12±1%).

α (°)	Unit, *n*	Compression						Tension					
		LT		*LR*		*TR*		*LT*		*LR*		*TR*	
0	*E* (MPa)	9196	(11.6)	8792	(10.4)	578	(29.6)	8446	(9.9)	8235	(12)	625	(2.7)
	n	7		10		9		9		9		9	
	ρ (g cm^{-3})	0.601	(5)	0.606	(3)	0.577	(4.2)	0.601	(5)	0.608	(3)	0.573	(3.8)
15	*E* (MPa)	7004	17	7023	(32.9)	602	(12.5)	6106	(12.2)	6305	(18)	574	(14.5)
	n	8		10		10		10		9		10	
	ρ (g cm^{-3})	0.617	(2.6)	0.617	(1.1)	0.617	(1.8)	0.612	(2.8)	0.617	(1.1)	0.617	(1.8)
30	*E* (MPa)	2403	4	2970	(7.8)	559	(7)	2966	(11.8)	2901	(7.9)	523	(5.5)
	n	9		10		10		9		10		10	
	ρ (g cm^{-3})	0.615	(2.3)	0.624	(2.1)	0.592	(1.4)	0.615	(2.3)	0.624	(2.1)	0.592	(1.4)
45	*E* (MPa)	1488	10	1684	(7.7)	463	(2.2)	1620	(11.5)	1694	(8.3)	433	(3.2)
	n	9		10		10		9		9		9	
	ρ (g cm^{-3})	0.622	(1.9)	0.611	(3.8)	0.554	(0.5)	0.623	(1.9)	0.614	(3.7)	0.553	(0.4)
60	*E* (MPa)	984	14.4	1185	(4.8)	663	(4.4)	1052	(18.7)	1155	(6)	655	(2.9)
	n	10		10		10		10		10		10	
	ρ (g cm^{-3})	0.652	(8.1)	0.617	(3.2)	0.599	(0.5)	0.652	(8.1)	0.617	(3.2)	0.599	(0.5)
75	*E* (MPa)	704	7.2	880	(3.6)	1002	(6.2)	740	(8.4)	849	(3.1)	995	(8.6)
	n	10		10		10		10		10		10	
	ρ (g cm^{-3})	0.608	(2.3)	0.597	(5.9)	0.603	(0.8)	0.608	(2.3)	0.597	(5.9)	0.603	(0.8)
90	*E* (MPa)	696	4.9	838	(2.9)	1143	(2.3)	637	(6.9)	866	(3.1)	1193	(3.9)
	n	9		10		9		10		10		9	
	ρ (g cm^{-3})	0.62	(1.8)	0.589	(0.7)	0.563	(1.4)	0.62	(1.8)	0.589	(0.7)	0.565	(1.4)

E_{ij} MOE for each orientation in MPa in the *ij*-plane where the *i*-orientation has an angle of 0° and the *j*-orientation has an angle of 90°; variation coefficient in % in brackets; ρ, raw density in g cm^{-3}; n, number of samples.

Table 2 MOEs for common ash from the literature.

		ρ (g cm^{-3})	ω (%)	E_L (MPa)	E_R (MPa)	E_T (MPa)
Pozgaj et al. (1997)	Compression	–	10–12	15,798	1875	1268
Niemz (1993)	–	0.69	12	13,000	1500	820
Hearmon (1948)	–	0.67	9	15,800	1510	800
Szalai (1994)	–	0.80	14	15,000	1640	970
Stamer (1935)	Compression	0.67	12	16,406	1567	833
Baumann (1922)	Compression	0.56–0.61	–	10,336	1669	1062
Baumann (1922)	Tension	0.56–0.61	–	8947	1590	1033

25% in the literature, which is not unusual for wood. The ratios between the individual directions do not spread in that magnitude. The mean ratio between *L*:*R*:*T* equals about 13.4:1.6:1.0, which is in accordance with our own measurements.

In Figure 3, the MOE from tension and compression tests are displayed in and between the anatomical directions. In general, the dependency of the MOE on the orientation is particularly pronounced. The modulus decreases to about one third of the maximum value up to 30° deflection from the *L* direction. In principle, the gradient can be described with the Hankinson's formula (Eq. 2), with an exponent of *n*=2.5 for the description of the obtained data in the *LT* plane, and 2.25 in the *LR* plane, for tension as well as for compression. The data for the *RT* plane are in good accordance with the fitted curve obtained by (Eq. 3) with the empirical factor *K*=0.4. The values of MOE in the main directions for calculation of the fit were taken from the results obtained in the individual plane.

An off-axis modulus minimum is revealed in the *RT* plane at about 45° between the *R* and *T* directions as demonstrated for common spruce by Garab et al. (2010), who compared experimental results with those calculated by a tensor transformation in the quest whether it is

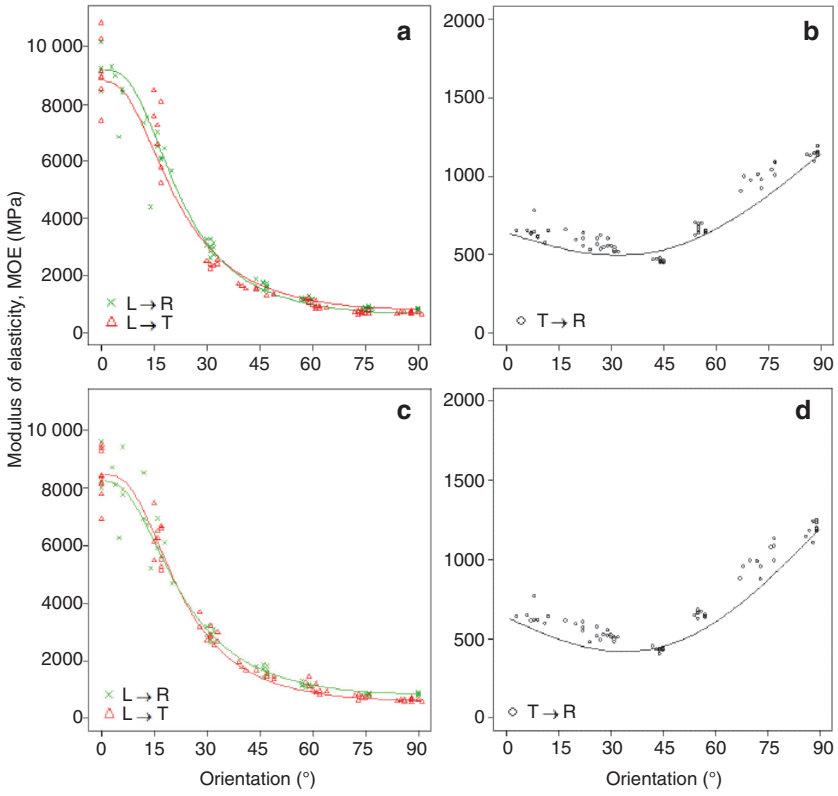

Figure 3 MOE in different planes under compression or tension load.
(a) Compression modulus from L to T direction. (b) Compression modulus from T to R direction. (c) Tension modulus from L to T direction. (d) Tension modulus from T to R direction.

admissible to treat the wood species as orthotropic materials. Lang et al. (2002) investigated several hardwood species by the same approach and found a significantly less distinctive anisotropy in the *RT* plane for all of them. The comparison and assessment of the common ash under consideration against the wood specific features of ring porous hardwood shows, however, a very similar behavior to spruce.

Poisson's ratio

The Poisson's ratios obtained in this research (Table 3) show typical occurrence for wood with the highest values in the *RT* plane, and the lowest values if the lateral extension is oriented in the *L* direction. In this case, caused by the minimal strain in the *L* direction, the measuring error has the most extensive influence on the result, evidenced by the high coefficient of variation. However, the method also revealed plausible results for these configurations. A statistically significant difference between tension and compression values is not detectable on the 5% level of significance. The only abnormality considering values from the literature (Table 4) is the Poisson's ratio in the *TL* configuration that is about twice as high as the own result.

Shear modulus

The results of shear moduli measurements (Table 5) reveal that the values G_{LR} and G_{RL} as well as the values G_{TR} and G_{RT} correspond to each other to a high degree, whereas the values of G_{TL} and G_{LT} reveal a remarkable difference, which is apparent by the higher variation coefficient for the *LT* plane. Significantly higher values were obtained if the load was applied in the *T* direction. Higher values were obtained in the *LR* than in the *LT* plane because of the reinforcing effect of the wood rays in the *R* direction. The ratio between *LR* to *LT* is about 1.2:1. Significantly lower values were obtained in the *RT* plane, because the geometry of the wood cells in this plane abets shear deformation. Comparison values of shear moduli in the literature reveal a high variation, caused by different methods used, variations in wood density, and further influencing factors. In the *LR* plane, the literature

Table 3 Results of Poisson's ratios for common ash.

	Units	TR		TL		RL		RT		LT		LR	
Compr.	ν (-)	0.58	(1.7)	0.21	(14.9)	0.30	(20.0)	0.36	(2.8)	0.05	(20.0)	0.04	(25.0)
	n	9		7		10		9		10		9	
	ρ (g cm^{-3})	0.601	(1.4)	0.563	(5.0)	0.606	(3.0)	0.577	(4.2)	0.589	(0.7)	0.629	(1.8)
	Ratio	14.5		5.25		7.5		9		1.25		1	
Tension	ν (-)	0.66	(4.6)	0.27	(37.0)	0.41	(7.3)	0.37	(5.4)	0.07	(14.3)	0.05	(20.0)
	n	9		9		9		9		10		10	
	ρ (g cm^{-3})	0.601	(1.4)	0.565	(5.0)	0.608	(3.0)	0.573	(3.8)	0.589	(0.7)	0.620	(1.8)
	Ratio	13.2		5.4		8.2		7.4		1.4		1	

Table 4 Poisson's ratios for common ash from the literature.

Literature		ρ (g cm^{-3})	ω (%)	ν_{TR}	ν_{TL}	ν_{RL}	ν_{RT}	ν_{LT}	ν_{LR}
Pozgaj et al. (1997)	–	–	–	0.73	0.57	0.51	0.47	0.06	0.04
Niemz (1993)	–	0.690	12	0.70	0.52	0.30	0.37	0.05	0.03
Hearmon (1948)	–	0.670	9	0.71	0.51	0.46	0.36	0.05	0.03
Hearmon (1948)	–	0.800	14	0.66	0.65	0.53	0.39	0.06	0.04
Stamer (1935)	Compression	0.670	9	0.71	0.51	0.46	0.36	0.05	0.03
Stamer (1935)	–	0.560	10	0.70	0.52	0.30	0.37	0.05	0.03

Table 5 Results of shear moduli for common ash.

Units (n)		LR		LT		TR	
G (MPa)	1468	(4.7)	1234	(16.5)	302	(6.2)	
n	22		24		18		
ρ (g cm^{-3})	0.616	(5.9)	0.601	(7.7)	0.617	(2.0)	
Ratio	4.9		4.1		1		

values are in the range between 860 and 1410 MPa, and measurements obtained in this study are nearly identical with the highest values obtained by Keunecke et al. (2008). The obtained results in the *LT* plane are clearly higher compared to the literature values (Table 6) that are caused by the extremely high values in the *TL* samples. In this plane, the literature values range from about 415 to 1030 MPa, however, a correlation between shear modulus and density is not evident. In the *RT* plane, the measured values are in between the literature data that range from about 270 to 511 MPa. The comparison of the results obtained on the front and back side of the specimens revealed nearly identical values with a mean coefficient of variation of about 3.8%.

3-D-description

Resulting from the obtained material properties, deformation bodies based on the work of Grimsel (1999), were created by a theoretical transformation of stress-strain equations to a 3-D coordinate system. Comparing the shape (Figure 4a) to displays of several different softwood and hardwood species by Grimsel (1999), Lang et al. (2002), Keunecke et al. (2008), Hering et al. (2012), and Ozyhar et al. (2012), only a small degree of anisotropy was visible in the case of ash; very comparable to the deformation bodies of beech or mahogany with the highest deformability in the *T* direction. Under torsion loading (Figure 4b),

Table 6 Shear moduli for common ash from the literature.

Literature	Method	ρ (g cm^{-3})	ω (%)	G_{LR} (MPa)	G_{LT} (MPa)	G_{TR} (MPa)
Stamer (1935)	–	–	9.2	1073	415	500
Hearmon (1948)	–	0.670	9	1340	890	270
Hearmon (1948)	–	0.800	14	860	619	250
Keunecke et al. (2008)	Ultrasound	0.648	–	1410	1030	511
Bucur (2006)	Ultrasound	0.670	–	1340	890	270

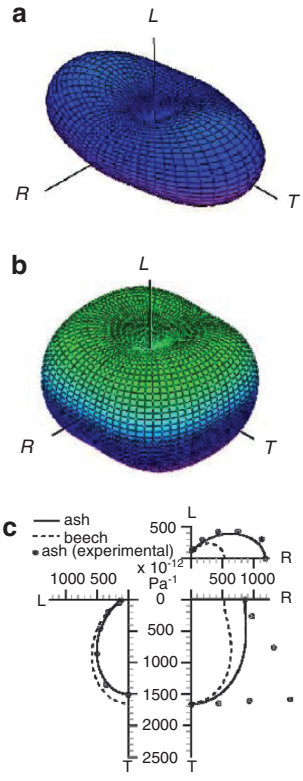

Figure 4 3-D compliance of common ash. (a) Deformation body under tension/compression load. (b) Deformation body under torsional load. (c) Polar diagrams for the principal planes under tension/compression load. Data for beech from Hering et al. (2012).

ash shows nearly isotropic behavior, also very comparable to the deformation bodies of the hardwoods like beech or mahogany. Comparing the theoretical results against stiffness measurements in the individual polar diagrams for the principal planes of anisotropy (Figure 4c), one significant inconsistency is visible in the *RT* plane. Here, the measurement result reveals a much stronger anisotropy compared to the theoretical compliance, which is significantly influenced by the shear modulus in the *RT* plane.

Conclusion

Compression, tension, and shear tests on common ash (*F. excelsior*), with various orientations of the fiber, and growth ring orientation were conducted. The off-axis MOE, shear moduli, and Poisson's ratios were obtained and used for a comparison of experimental and theoretical data based on tensor transformations. The dependency on the fiber direction obtained by the experiments coincided well with the calculated deformations in the off-axis fiber angles, however, ash showed a significantly higher degree of anisotropy in the *RT* plane compared to the estimated curve progression. It is anticipated that the ring porous structure of ash with its density variations along the annual ring progression reveals a similar result as found for softwoods such as spruce.

Acknowledgments: The authors thank Mr. Thomas Schnider for his accurate preparation of the specimens and Dr. Stefan Hering for his support with the tensor trasformation algorithms.

Received September 29, 2013; accepted March 24, 2014; previously published online May 9, 2014

References

Arcan, M., Hashin, Z., Voloshin, A. (1978) A method to produce uniform plane-stress states with applications to fiber-reinforced materials. Exp. Mech. 18:141–146.

Baumann, R. (1922) Die bisherigen Ergebnisse der Holzprüfungen in der Materialprüfungsanstalt an der TH Stuttgart. Verlag des Vereins Deutscher Ingenieure, Berlin.

Bodig, J., Jayne, A. Mechanics of Wood and Wood Composites. Krieger Publishing Company, 1993.

Bonoli, C., Niemz, P., Mannes, D. (2005) Investigation into certain mechanical properties of ash. Schweizer Zeitschr. Forstwesen. 156:432–437.

Bucur, V. Acoustics of Wood. 2nd edn, Springer-Verlag, Berlin, Heidelberg, Germany, 2006.

DIN 68364 (2003) Properties of wood species – Density, modulus of elasticity and strength, Beuth-Verlag, Berlin.

Garab, J., Keunecke, D., Hering, S., Szalai, J., Niemz, P. (2010) Measurement of standard and off-axis elastic moduli and Poisson's ratios of spruce and yew wood in the transverse plane. Wood Sci. Technol. 44:451–464.

Grimsel, M. (1999) Mechanisches Verhalten von Holz: Struktur- und Parameteridentifikation eines anisotropen Werkstoffes. Dissertation, Dresden, p. 89.

Goldenberg, N., Arcan, M., Nicolau, E. (1958) On the most suitable specimen shape for testing shear strength of plastics. International Symposium on Plastics Testing and Standardization, Am. Soc. Testing Mats. 247:115–121.

Hearmon, R. The elasticity of wood and plywood. HM Stationery Office London, 1948.

Hearmon, R.F., Barkas W.W. (1941) The effect of grain direction on the Young's moduli and rigidity moduli of beech and Sitka spruce. Proc. Phys. Soc. 53:674–680.

Hering, S., Keunecke, D., Niemz, P. (2012) Moisture-dependent orthotropic elasticity of beech wood. Wood Sci. Technol. 46:927–938.

Hörig, H. (1933) Zur Elastizität des Fichtenholzes. 1. Folgerungen aus Messungen von H. Carrington an Spruce. Z. Tech. Phys. 12:369–379.

Hung, S.C., Liechti, K.M. (1999) Finite element analysis of the arcan specimen for fiber reinforced composites under pure shear and biaxial loading. J. Compos. Mater. 33:1288–1317.

Iosipescu, N. (1967) New accurate procedure for single shear testing of metals. J. Mater. 2:537–566.

Kabir, M.F., Sidek, H.A., Daud, W.M., Khalid, K. (1997) Effect of moisture content and grain angle on the ultrasonic properties of rubber wood. Holzforschung. 51:263–267.

Kennedy, R.W. (1968) Wood in transverse compression. For. Prod. J. 18:36–40.

Keunecke, D., Hering, S., Niemz, P. (2008) Three-dimensional elastic behaviour of common yew and Norway spruce. Wood Sci. Technol. 42:633–647.

Kollmann, F. Die Esche und ihr Holz. Verlag Julius Springer, Berlin, 1941.

Kollmann, F. Technologie des Holzes und der Holzwerkstoffe. Springer, Berlin, 1951.

Kühne, H. Untersuchung über einige Eigenschaften des Eschen- und Robinienholzes im Hinblick auf dessen Verwendbarkeit für Werkzeugstiele. Forschungsbericht Empa, 1951.

Lang, E.M., Bejo, L., Szalai, J., Kovacs, S., Anderson, R.B. (2002) Orthotropic strength and elasticity of hardwoods in relation to composite manufacture. Part II. Orthotropy of compression strength and elasticity. Wood Fiber Sci. 34:350–365.

Leclerco, A. (1975) La qualité du bois de frêne. Bull. rech. Agron. Gembloux. 10:497–526.

Liu, J.Y. (2002) Analysis of off-axis tension test of wood specimens. Wood Fiber Sci. 34:205–211.

Neuhaus, F.H. (1983) Über das elastische Verhalten von Fichtenholz in Abhängigkeit von der Holzfeuchtigkeit. Holz Roh. Werkst. 41:21–25.

Niemz, P. Physik des Holzes und der Holzwerkstoffe. DRW-Verlag, Leinfelden-Echterdingen, 1993.

Ozyhar, T., Hering, S., Niemz, P. (2012) Moisture-dependent elastic and strength anisotropy of European beech wood in tension. J. Mater. Sci. 47:6141–6150.

Pozgaj, A., Chovanec, D., Kurjatko, S., Babiak, M. (1997) Struktura a vlastnosti drevna. Priroda. Bratislava.

Reiterer, A., Stanzl-Tschegg, S.E. (2001) Compressive behaviour of softwood under uniaxial loading at different orientations to the grain. Mech. Mater. 33:705–715.

Sell, J. Eigenschaften und Kenngrössen von Holzarten. Baufachverlag, Dietikon, 1997.

Sliker, A., Yu, Y. (1993) Elastic constants for hardwoods measured from plate and tension tests. Wood Fiber Sci. 25:8–22.

Stamer, J. (1935) Elastizitätsuntersuchungen an Hölzern. Archive of Applied Mechanics. 1:1–8.

Suzuki, H., Sasaki, E. (1990) Effect of grain angle on the ultrasonic velocity of wood. Mokuzai Gakkaishi 36:103–107.

Szalai, J. Anisotropic behaviour of wood and wood based materials (in Hungarian). Hillebrand Nyomda Kft., Sopron, 1994.

Voigt, W. Lehrbuch der Kristallphysik. B.G. Teubner, Leipzig, 1928.

Wagenführ, R. Holzatlas. Fachbuchverlag, 4th edn, Leipzig, 1996.

Wommelsdorf, O. Dehnungs- und Querdehnungszahlen von Hölzern. Dissertation, Technische Hochschule Hannover, 1966.

Xavier, J., Oliveira, M., Morais, J., Pinto, T. (2009) Measurement of the shear properties of clear wood by the Arcan test. Holzforschung 63:217–225.

Yoshihara, H. (2009) Prediction of the off-axis stress strain relation of wood under compression loading. Eur. J. Wood Prod. 67:183–188.